Original scientific paper

Annealing effect on structural and electrochemical performance of Ti-doped LiNi$_{1/3}$Mn$_{1/3}$Co$_{1/3}$O$_2$ cathode materials

Kelimah Elong[1,2], Muhd Firdaus Kasim[1,2,✉], Nurhanna Badar[3], Norashikin Kamarudin[1], Norlida Kamarulzaman[1] and Zurina Osman[4]

[1]*Centre for Functional Materials and Nanotechnology, Institute of Science, Universiti Teknologi MARA, 40450 Shah Alam, Malaysia*

[2]*School of Chemistry and Environment, Faculty of Applied Sciences, Universiti Teknologi MARA, 40450 Shah Alam, Malaysia*

[3]*Faculty of Science and Marine Environment, Universiti Malaysia Terengganu, 21030 Kuala Nerus Terengganu, Malaysia*

[4]*Physics Department, Universiti Malaya, 50603, Kuala Lumpur, Malaysia*

Corresponding author: ✉*muhdfir@uitm.edu.my*

Abstract

NMC 111 cathode materials exhibit engaging properties in high energy density and low cost, making it great potential for the next generation of high-energy lithium-ion batteries. However, it still faces challenges such as fast capacity fade, especially at high C rates. Herein, we implement the novel Ti-doped cathode material, LiNi$_{0.3}$Mn$_{0.3}$Co$_{0.3}$Ti$_{0.1}$O$_2$ (NMCT) synthesized via the combustion method. It was discovered that NMCT can effectively improve capacity delivery at high C rates. The T80 material demonstrated superior electrochemical annealed at 800 ˚C for 72 h, with an exceptional specific discharge capacity of 148.6 mAh g^{-1} and excellent cycle stability (capacity retention 96.8 %) after 30th cycles at 3 C. The results demonstrated that Ti-doped NMC had superior advantages for LiNi$_{1/3}$Mn$_{1/3}$Co$_{1/3}$O$_2$ (NMC 111) material at the optimum temperature of 800 °C for 72 h. It is one of the potential cathode materials for Li-ion batteries.

Keywords
Cathode material; Ti doping; combustion method; rietveld refinement, Li-ion battery; NMC 111

Introduction

The world's fastest-growing battery technology is Li-ion batteries (LIBs), which are widely used in the application of portable electronics, mobile phones, power tools, and electric vehicles (EVs). In LIBs, it is important to secure stable cathode materials as they govern the capacity of the whole cell. LiNi$_{1-x-y}$Mn$_x$Co$_y$O$_2$ (NMC), LiNi$_{1-x-y}$Co$_x$Al$_y$O$_2$ (NCA) and LiFePO$_4$ (LFP) are currently three cathode active

materials that constitute a majority use in LIBs [1]. Among the most widely investigated cathode materials, NMC is well-investigated, showing improved structural/thermal stability and cycling performance [2].

NMC is an attractive cathode material, as it combines the advantages of LiCoO$_2$ (high energy density), LiNiO$_2$ (high reversible capacity), and LiMnO$_2$ (high thermal stability) [3]. This material has better characteristics such as high capacity, less toxicity, and low cost compared to commercial LiCoO$_2$ material [4]. No wonder that two NMC compositions which are LiNi$_{1/3}$Mn$_{1/3}$Co$_{1/3}$O$_2$ (NMC 111) and LiNi$_{0.5}$Mn$_{0.3}$Co$_{0.2}$O$_2$ (NMC 532), already used in the commercialization of lithium batteries [5]. Although there are a large number of reports covering the properties of specific NMC composition, the challenges remain. It still has limitations, especially for EVs applications, due to poor rate capability and higher degradation at high voltage [6], which are its main impediments to comercialization. Therefore, batteries researchers have proposed some methods for the modification of NMC cathode, such as morphology control, use of electrolyte additives, ion doping, surface modification, etc., to remedy this drawback so that the properties, including high power and high energy densities, can be improved.

As is widely known, different methods and process parameters play a vital role in the crystal structure, morphology, crystallite size, and electrochemical performance of the cathode materials [7]. Many alternative methods have been used to prepare the NMC powders, such as the solid-state method [8], sol-gel method [9], co-precipitation method [10], spray pyrolysis [11], and so on. It is difficult to synthesize homogenous NMC materials, so selecting a suitable preparation method is important to obtain pure and single-phase final products that will give the optimum electrochemical performance. One of the effective methods that can be used is the combustion method. This method is simple, low cost eco-friendly, giving high crystalline phases and better control of the microstructures, which will influence the electrochemical performance [12]. Zhao *et al.* [13] reported that NMC111 synthesized *via* combustion can achieve a high discharge capacity of 179.2 mAh g^{-1} due to the high crystallinity and small particle sizes.

Element doping plays a critical role in stabilizing the structure and each transition metal added to the crystal structure of NMC has a distinct role. Changes in the oxidation state of Ni from Ni^{2+} to Ni^{3+} and to Ni^{4+} help in improving the capacity [14]. After the Ni^{2+} oxidation, Co will oxidize from Co^{2+} to Co^{3+} to prevent the Ni from drifting to the Li sites, which causes less cation mixing between Li$^+$/Ni^{2+} ions [15]. Mn^{4+} ions are responsible for maintaining structural integrity and reducing production costs by replacing cobalt with cheaper manganese [16]. There are several elements used as dopants, such as aluminium (Al), iron (Fe), tin (Sn), chromium (Cr), zirconium (Zr), copper (Cu), magnesium (Mg), and titanium (Ti). Eilers-Rethwisch *et al.* [17] reported that capacity fading is reduced when Al, Fe, and Sn were used as dopants. Zheng *et al.* [18] proved that doping with Al shows a higher specific discharge capacity of NMC 111, which is 154.9 mAh g^{-1}. This is due to the good crystallinity and homogeneous distributions of smaller particles size that provide higher surface area. However, Samarasingha *et al.* [19] reported that the X-Ray diffraction pattern of Al dopant showed the existence of secondary phase impurity with lower specific discharge capacities of 120 mAh g^{-1}. Thus, it is very important to choose the right dopant to improve the structural integrity, leading to excellent electrochemical performance.

Wang *et al.* reported Ti doping improved the cycling performance of the Li$_{1.2}$Mn$_{0.54-x}$Ti$_x$Ni$_{0.13}$Co$_{0.13}$O$_2$ cathode material by enhancing the framework between electrode/electrolyte interface stability [20]. Ti used as a dopant in NMC 811 also showed much better cycling and rate property with a cut-off potential of 4.3 V [21]. Table 1 summarizes the electrochemical properties of NMC from the previous

works. To the best of our knowledge, no study of Ti dopant in NMC 111 prepared using the combustion method. Therefore, in this paper, we aim to understand the impact of novel partial substitution of Ti in $LiNi_{1/3}Mn_{1/3}Co_{1/3}O_2$ material on the phase, structure, morphology, size of the crystallite, element distribution, and electrochemical performances of the materials with increasing the annealing temperature that synthesizes using combustion method.

Table 1. *A comparison of electrochemical performance of previously reported NMC materials*

Materials	Synthesis method	Current density, mA g^{-1}	Voltage range, V	Initial discharge capacity, mAh g^{-1}	Cycle number	Final capacity, mAh g^{-1}	Capacity retention, %	Ref.
NMC 111	Sol-gel	2.0	2.5- 4.5	187.7	50	80.9	43.1	[22]
NMC 111	Solvothermal	1.0	2.5 - 4.5	154.1	500	73.3	52.43	[23]
NMC 111	Wet-chemical	1.0	3.0 - 4.3	143.0	100	130.4	91.2	[24]
NMC 111	Solid State	1.0	2.8 - 4.3	157.7	100	151.1	95.8	[25]
Ti-doped NMC 111	Co-precipitation	0.2	3.0 - 4.3	153.6	50	152.7	99.41	[26]
Ti-doped NMC 811	Solid state reaction	0.1	2.8 - 4.3	180.7	100	160.3	88.71	[21]
Ti-doped NMC 532	Solid state reaction	1.0	2.8 - 4.6	184.3	200	172.7	93.4	[27]

Experimental

Synthesis of cathode materials

In a typical process, raw materials employed in the experiment were lithium nitrate, $LiNO_3$, nickel(II) nitrate hexahydrate ($Ni(NO_3)_2 \cdot 6H_2O$), manganese(II) nitrate hexahydrate, $Mn(NO_3)_2 \cdot H_2O$, cobalt(II) nitrate hexahydrate, $Co(NO_3)_2 \cdot 6H_2O$ and titanium(IV) methoxide, $Ti(OCH_3)_4$. All starting materials were weight according to the stoichiometric proportion of $LiNi_{0.3}Mn_{0.3}Co_{0.3}Ti_{0.1}O_2$ (NMCT). $LiNO_3$, $Ni(NO_3)_2 \cdot 6H_2O$, $Mn(NO_3)_2 \cdot H_2O$, and $Co(NO_3)_2 \cdot 6H_2O$ were first dissolved in an appropriate amount of deionized water and $Ti(OCH_3)_4$, was dissolved in nitric acid, HNO_3 to form titanium nitrate. The equation for the reaction is given by the following expression, equation (1):

$$Ti(OCH_3)_4 + 4HNO_3 \rightarrow Ti(NO_3)_4 + 4CH_3OH \tag{1}$$

After that, all starting raw materials were mixed in a 1 L beaker. The citric acid, $C_6H_8O_7$, was added to the solution as a fuel and the mixture was uniformly mixed by stirring for 1 hour. The solution was heated slowly at 200 °C on a hot plate to give auto-combusted powders. Finally, the powders were calcined under various temperatures for 72 hours to obtain the target NMCT cathode material and then subjected to further analyses. Finally, NMCT materials annealed at 650, 700, 750, 800, 850 and 900 °C for 72 hours were denoted as T65, T70, T75, T80, T85, and T90, respectively. The synthesis process is illustrated in Figure 1.

Characterization

The phase composition and structural characteristics of all samples were studied with X-ray diffraction (XRD, PANalytical Xpert Pro diffractometer) with Cu Kα radiation and X'celerator detector. The measurement data were collected over the range of 10° < 2θ < 90° with a step size of 0.02°. The crystal structure was analyzed by the Rietveld refinement using X'pert Highscore Plus Software. The XRD pattern for Rietveld refinement was carried out at a higher count up to 10,000 at 2θ range 10 to 151°.

Field emission scanning electron microscope (FESEM, JEOL JSM-7600F) equipped with an energy dispersive X-ray spectroscopy (EDX, Oxford INCA X-Max 0021) was used for analyzing the morphology, element distribution, and composition mapping.
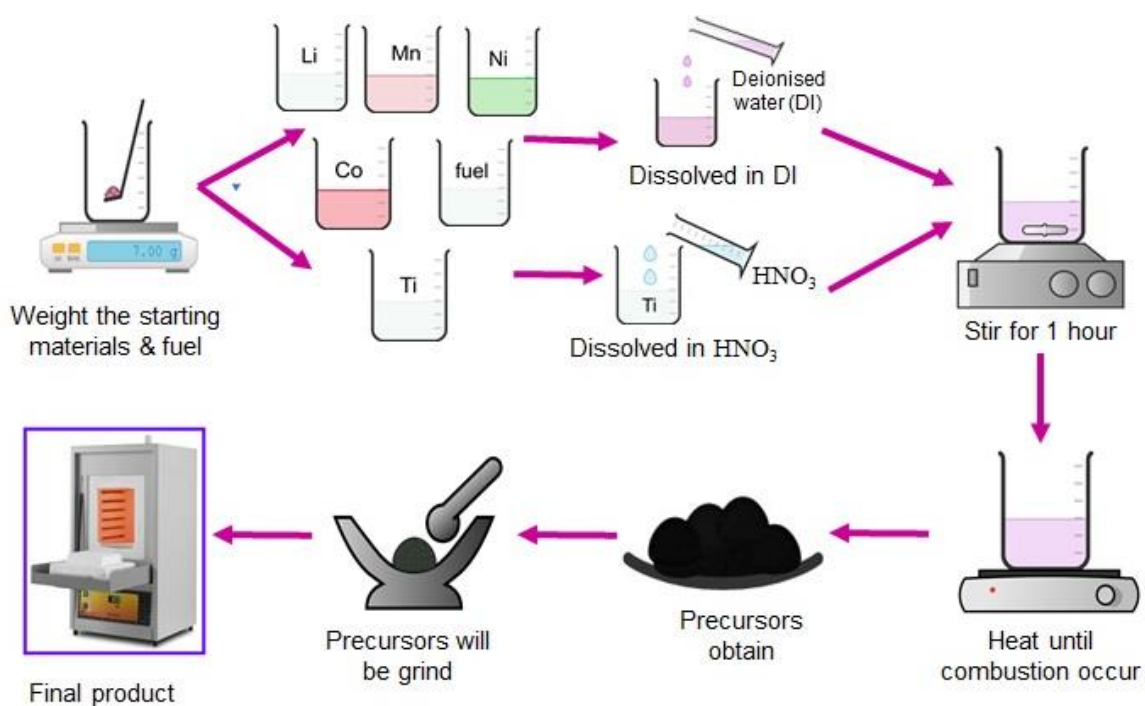
Figure 1. *Summary of combustion method*

The microstructural characteristics of the material were assessed by high-resolution transmission electron microscopy (HRTEM, TEM JEOL 2100) at 200 kV. For the preparation, the sample was mixed with methanol and treated with ultrasound for 1 hour. The suspension was deposited onto standard C/Cu grids and heated in the oven for 1 hour at 80 °C.

Electrochemical measurements

Active LiNi$_{0.3}$Mn$_{0.3}$Co$_{0.3}$Ti$_{0.1}$O$_2$ (NMCT) material, polytetrafluoroethylene (PTFE) binder, and Super P with the mass ratio of 8:1:1 were well mixed to prepare the working electrode. The mixture was pressed onto a stainless-steel grid and dried in an oven at 200 °C for 24 hours. The cell was assembled in a dry glove box (Unilab Mbraun) under an Ar atmosphere (O$_2$ < 0.1 ppm, H$_2$O < 0.1 ppm) with pure lithium foil as the counter electrode and Celgard 2400 microporous as the separator. The electrolytes are 1 M LiPF$_6$ dissolved in a 1:1:1 (v/v/v) mixture of dimethyl carbonate (DMC), ethyl methyl carbonate (EMC), and ethylene carbonate (EC). The cyclic voltammetry (CV) was performed between 0.5 - 5.6 V with a scan rate of 3 mV s^{-1}. Galvanostatic charge-discharge tests were conducted using Wonatech (WBCS 3000) battery tester at 43.5 mA g^{-1} current density in the voltage range of 2.5 - 4.2 V.

Results and discussion

Phase and structural studies

The effect of calcination temperature on the formation of NMCT is investigated using XRD patterns shown in Figure 2. The main peaks of all samples are well indexed and isostructural with a typical hexagonal layered α-NaFeO$_2$ structure (ICDD pattern number 01-070-2685 for lithium cobalt oxide) except for T85 and T90 materials. The presence of cobalt oxide (Co$_3$O$_4$) peak at 30.9° made both samples cannot be used for further other characterization and also electrochemical measurement [28]. T65 material shows low-intensity peaks, which indicate low crystallinity, but with the increase in the calcination temperature, the intensities of all peaks increase and the peaks become sharper, especially for T80 material that reflects the increase of the crystallinity that expected will give good electrochemical performance [29].

To further investigate the effect of temperatures on the crystal structure, we calculated the ratio of (003) and (104) peaks called RIR in Table 2, which indicates the degree of "layeredness". All samples show an RIR value over 1.2 and slightly increase with increasing calcination temperature, indicating a good crystallinity and lower cation mixing in NMCT samples. RIR > 1.2 is important for layered cathode material with a well-ordered structure with limited Li/Ni mixing [2]. T80 material gives the positive sign of good cation ordering and crystallinity when demonstrated with the highest $I_{(003)}/I_{(104)}$ ratio [30]. It also causes a clear split between (006) and (102) peaks and good symmetry of the (108) and (110) peaks (in the circle zone of Figure 2(d)), which indicates this material has a well-defined layered structure. The R-factor, which is defined as $(I_{(006)} + I_{(102)})/ I_{(101)}$, should be at a minimum in a system with good hexagonal ordering [31]. These results prove that the crystal structure of NMC 111 did not change with Ti incorporation and increased calcination temperature promotes the formation of a well-defined layered structure.

To further analyze the effect of temperature on NMCT materials, all materials except T85 and T90 were analyzed by Rietveld refinement. The XRD pattern for Rietveld refinement, as shown in Figure 3, was carried out at a higher count up to 10,000 at 2 θ range 10 to 151˚. The summary of crystallographic values is listed in Table 2. The confidence profile factor, R_{wp} shows the refinement results of NMCT were credible (less than 10 %), indicating the results of the Rietveld refinements have a good fitting degree [32]. All the materials show the ratios of the lattice constants, c/a values are larger than 4.9, representing that the NMCT materials have a good hexagonal layered structure [33]. T65 material shows a c/a value of 4.9743, as the temperature increase, the crystallographic values of c/a ratio and volume (V) gradually enhance, corroborating that Ti was incorporated into the NMC crystal lattice [21]. It was found that T65 has the largest c-axis compared to other samples, which supposedly gives an advantage for Li ions to diffuse easier [34], but unfortunately, this material has the highest cation mixing, which about 10 % of Ni^{2+} takes place at the Li^+ 3a site. Refinement reveals that the c-axis was decreased when temperature increased except for the T80 sample. It was also found that, as the temperature increased, the cation mixing decreased. Interestingly, the T80 sample possesses a larger c-axis and the lowest cation mixing of 6.8 % as compared to other samples. By having good structural integrity, it is believed that this material will have excellent electrochemical performance. Refinements results prove that increasing annealing temperature can help promote the formation of a well-defined layered structure that allows Li+ ions to move randomly between the layered cathode materials, subsequently improving the cathode's electrochemical performance materials [35].

The atomic distance of Li-O, Li-TM, and TM-O obtained from refinements is shown in Table 2, where TM indicates transition metal. Based on the outcome, increasing temperature shows the materials had a shorter bond length of Li-O, a larger atomic distance of Li-TM, and a longer bond length of TM-O. It can see that T65 has a larger atomic distance and longer bond length, but the material has a higher level of cation mixing than shown by the RIR value. This may be one of the reasons why T65 does not show good electrochemical charge-discharge, as seen later. Interestingly, the T80 sample has a larger atomic distance of Li-O and TM-O, and in addition to that, this material has the smallest cation mixing as compared to other samples. By having a larger atomic distance of Li-O, less energy is needed for Li-ions to break free from their position in the crystal structure, which could promote more Li-ions diffusion, which later gives a higher specific capacity for the material to hold [36]. Therefore, T80 is estimated to exhibit better electrochemical performance due to atomic distance and RIR value.
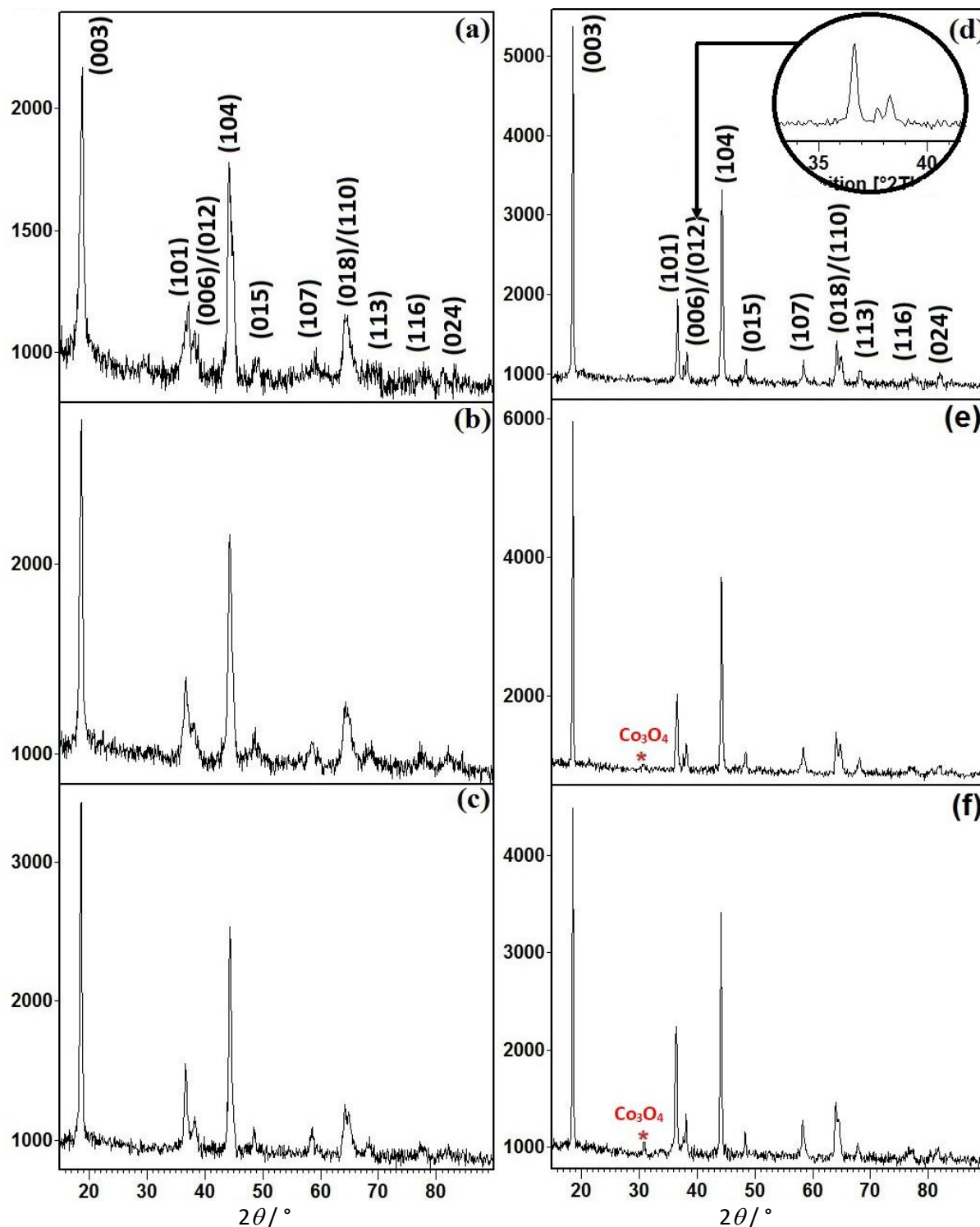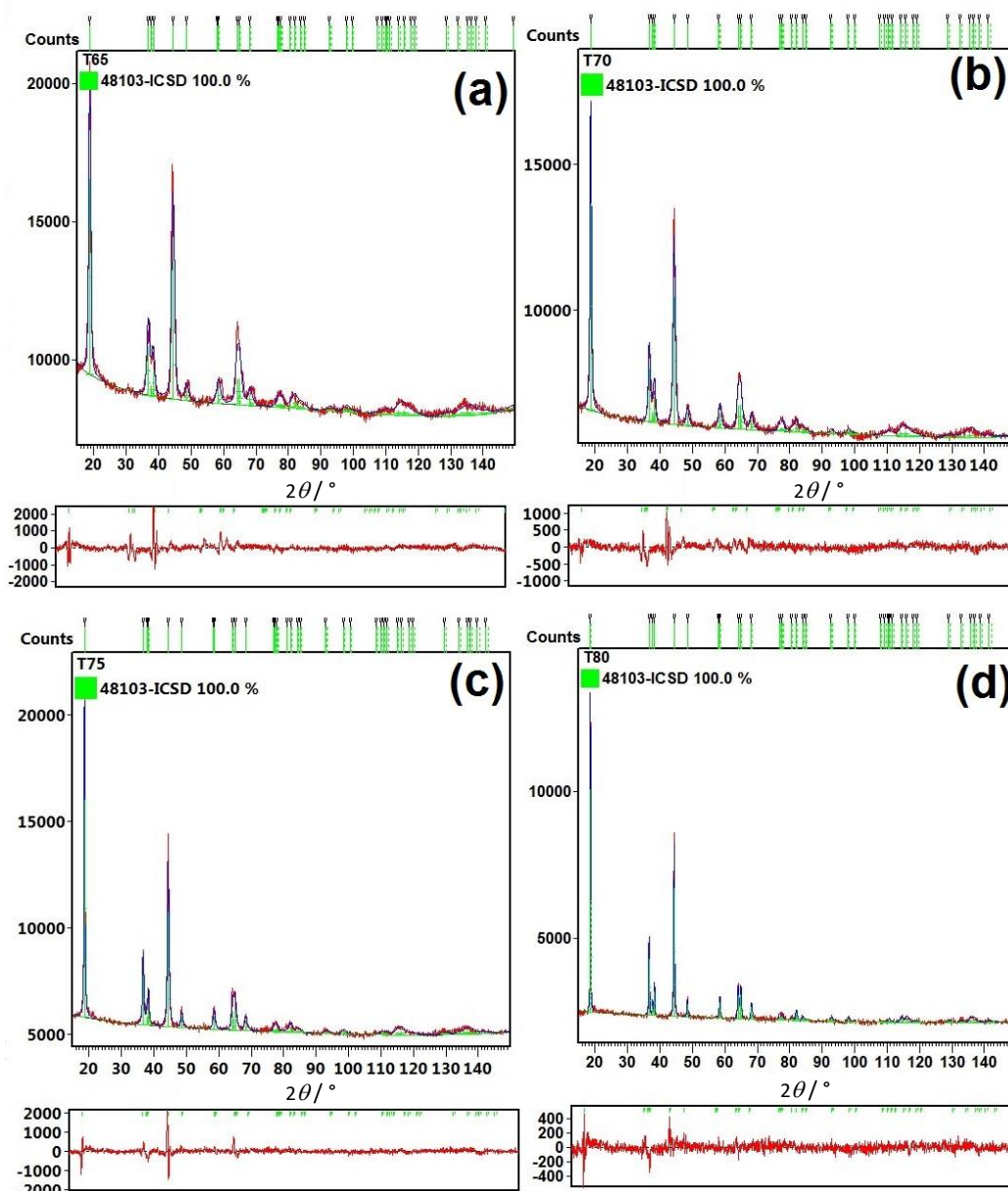
Figure 2. *XRD patterns of (a) T65 (b) T70 and (c) T75 (d) T80 (e) T85 and (f) T90*

Table 2. *Crystallographic parameters of NMCT materials annealed at different temperatures (SOF - site occupancy factor)*

Sample	$a = b$ / Å	c / Å	V / Å^3	c/a	R_w	SOF						Bond length, Å			RIR*
						Co 3b	Ni 3b	Ni 3a	Ti 3b	Mn 3b	O 16c	Li-O	Li-TM	TM-O	
T65	2.8774	14.3130	102.8434	4.9743	2.0354	0.3218	0.2270	0.1063	0.0925	0.3252	1.0000	2.139	2.911	1.962	1.34
T70	2.8651	14.2428	101.2548	4.9711	1.8968	0.3225	0.2406	0.0927	0.0924	0.3253	1.0000	2.127	2.893	1.952	1.44
T75	2.8621	14.2324	101.8540	4.9727	2.2172	0.3238	0.2532	0.0801	0.0930	0.3261	1.0000	2.125	2.890	1.950	1.52
T80	2.8690	14.2883	101.8920	4.9802	2.2468	0.3226	0.2653	0.0680	0.0921	0.3252	1.0000	2.132	2.901	1.955	1.80

*$I_{(003)}$ / $I_{(104)}$

Figure 3. *Rietveld refinements of XRD patterns of (a) T65, (b) T70, (c) T75 and (d) T80*

Morphology

Morphology and particle size are one of the main effects that can affect the electrochemical performance of cathode materials. The SEM images of the NMCT materials at 30000 magnification are shown in Figure 4(a-d). The materials have a spherical shape with some polyhedral-type and smooth crystals. As the calcination increase, the average crystallite sizes become larger, significant to the crystal growth, and the distribution of particle size more uniform when increasing the temperature. The average crystallite size for all the samples was measured *via* FESEM images by randomly measuring 80 crystallites, as shown in Table 3. From Figure 4(e), we can see that the crystallite size distribution of the T80 sample approximates to the normal distribution and agrees with the average crystallite size of 155.57 nm shown in Table 3. The EDX spectra in Figure S-1 (Supplementary Material) indicate the presence of all elements in the materials, and the chemical quantification of Ni, Mn, Co, and Ti are given in the spectra.
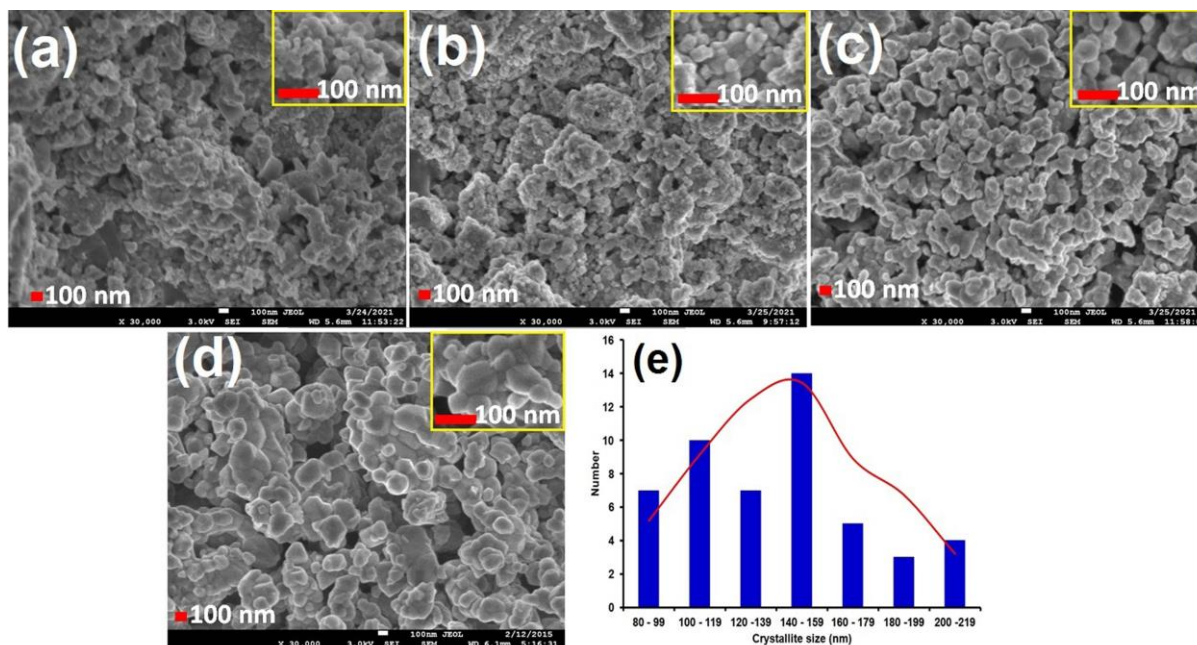
Figure 4. *SEM image of (a) T65 (b) T70 (c) T75 (d) T80 and (e) average crystallite size of T80*

Due to the excellent structural integrity possessed by the T80 sample (Table 2), this material was then subjected to the TEM studies and the results are shown in Figure 5. In Figure 5(a), it is clear that the morphology and crystallite size of the T80 sample from the TEM micrograph agree with the SEM results. A high-resolution image of the T80 nanocrystals is shown in Figure 5(b) for lattice studies, where the selected spot used can be seen from the marked circle in Figure 5(a). The higher magnification image clearly shows the T80 nano crystal's lattice, demonstrating that the T80 sample is crystalline in nature with a single crystalline structure, indicating atomic distribution with high ordering.
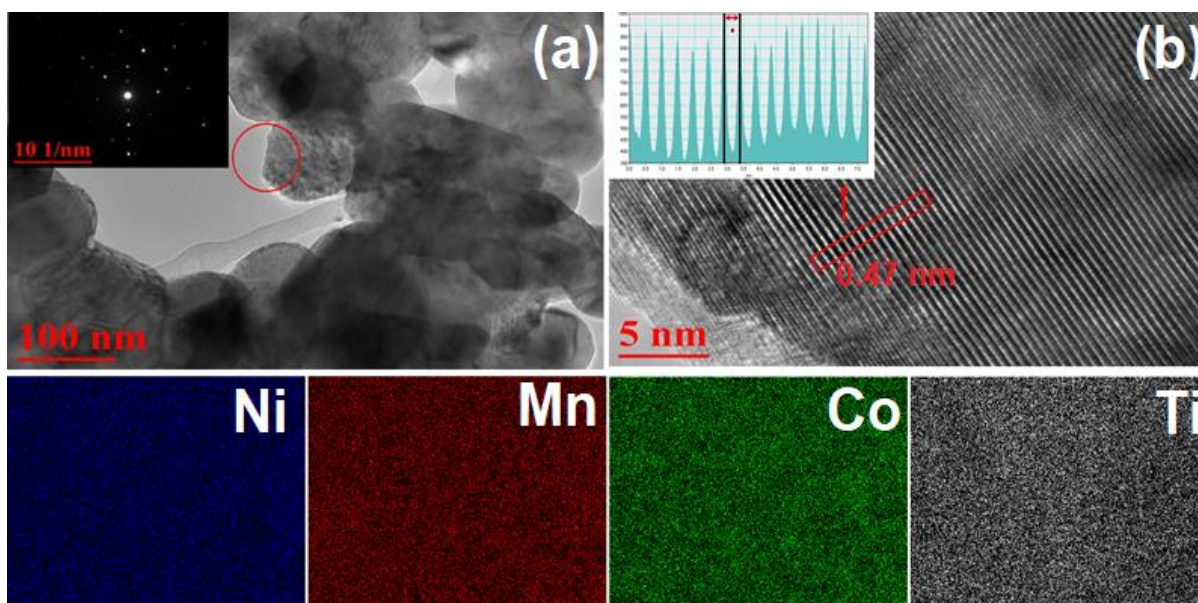

Figure 5. *TEM image of (a) T80 (b) HRTEM image of T80 in the circle zone of and corresponding element mapping of a T80 material*

Good crystal structure and orderly atomic distribution are speculated to facilitate the electrochemical performance of the NMCT [23]. The HRTEM image of the T80 nano crystal marked by the rectangle zone in Figure 5(b) displays an interplanar distance of 0.47 nm, which corresponds

to the (003) plane spacing of NMC [37]. The (003) crystal plane is identified using the selected area FFT results (inset image in Figure 5(a)). The existence of (003) crystal plane also confirms the hexagonal layered α-NaFeO$_2$ structure of the T80 nanocrystal as revealed by the XRD data.

EDS mapping of T80 material manifested in Figure 5 reveals the presence of nickel (blue), cobalt (green), manganese (red), and titanium (grey), respectively. Overall, the area distribution of all elements was fully uniform on the surface of the material and the effective incorporation in the particles.

Table 3. *The crystallite size and cyclic voltammetry of LiNi$_{0.3}$Mn$_{0.3}$Co$_{0.3}$Ti$_{0.1}$O$_2$ cathode materials*

Cathode material	Crystallite size range, nm	Average crystallite size nm	$E_{Oxidation}$ / V	$E_{Reduction}$ / V	ΔE / V
T65	47 - 113	80.34	5.59	3.11	2.48
T70	56 - 143	100.68	5.24	2.61	2.63
T75	53 - 263	134.8	5.59	2.71	2.88
T80	103 - 268	155.57	4.78	3.26	1.52

Electrochemical performance of cathode materials

Cyclic voltammetry (CV) was a measure to study the redox potential of the transition metal ions in NMCT. Figure 6(a) shows the CV curves in which lithium metal is used as the counter and reference electrodes. The broad peak between 4.78 V to 5.60 V on the charge curve has been ascribed to the oxidation of Co ions (Co^{3+}/Co^{4+}) and Ni ions (Ni^{2+}/ Ni^{4+}), accounting for the Li$^+$ extraction from the cathode material. The reduction peak between 2.71 V to 3.26 V on the discharge curve illustrates the reduction of Co ions (Co^{4+}/Co^{3+}) and Ni ions (Ni^{4+}/ Ni^{2+}), which means that Li$^+$ insert back into the layered material [38].
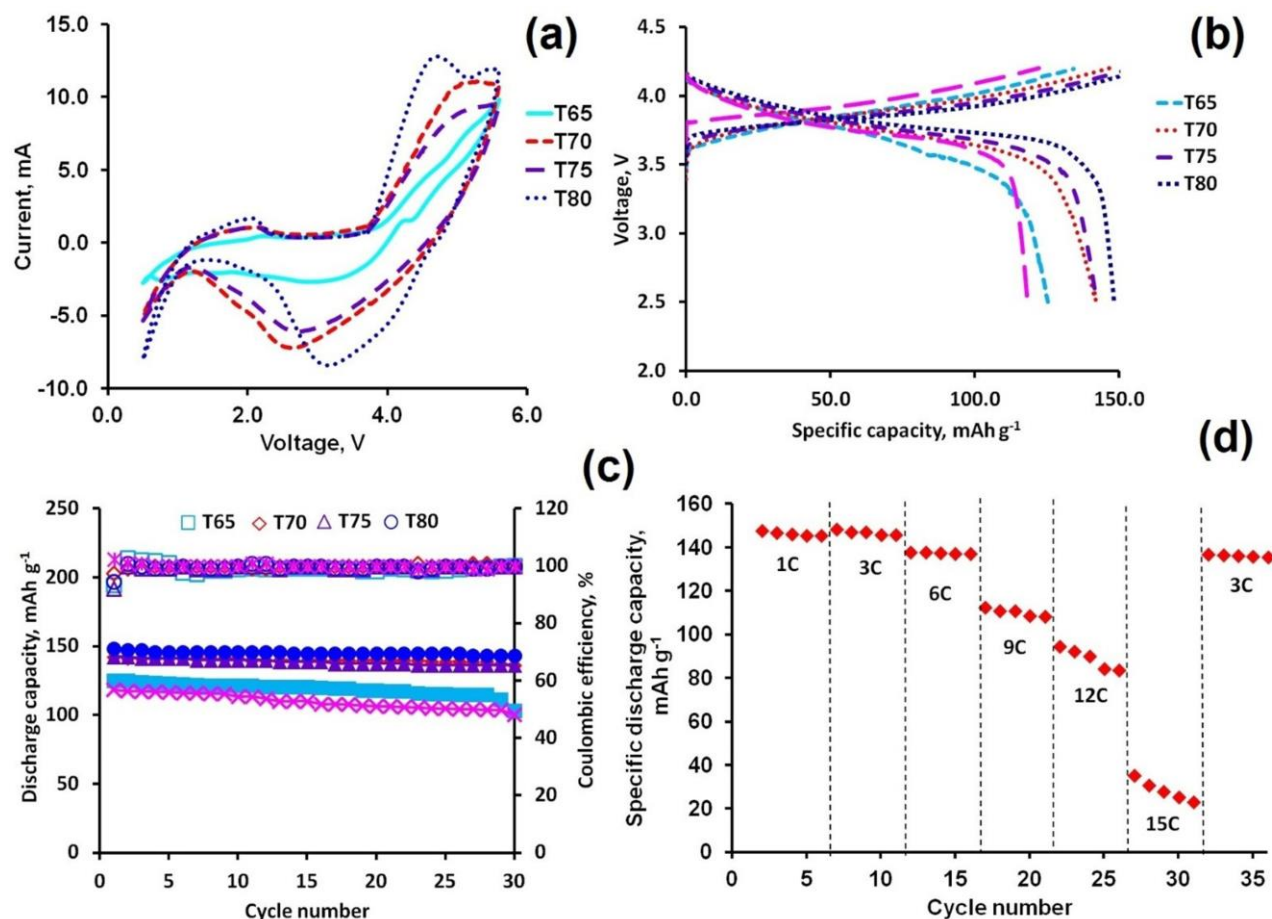
Figure 6. *(a) Cyclic voltammetry, (b) 1st charge discharge capacity (c) cyclability and (d) comparison of cycling performance vs. C-rates for T80 material*

The potential difference, ΔE ($E_{\text{oxidation}} - E_{\text{reduction}}$) was calculated to explain the cycle reversibility of the electrode of NMCT. ΔE value was increased with the increasing annealing temperature but not for T80 and the details are revealed in Table 3. This material shows smaller ΔE and higher peak currents indicating better electrode reaction kinetics and rate performance [39]. This may be one of the reasons why T80 material shows good electrochemical performance, as seen later.

Within the voltage range, it is worth pointing out that the performance of NMCT materials is comparable to the reported in the literature [40,41]. As shown in Figure 6(b), the best material, T80 exhibited the highest 1$^{\text{st}}$ discharge specific capacity of about 148.6 mAh g^{-1}. This seemed to be consistent with the good cation ordering shown by XRD analysis. Overall, NMCT materials demonstrated superior electrochemical after 30$^{\text{th}}$ cycles shown in Table 4 and Figure 6(c), especially T80 material with a higher discharge capacity of 143.7 mAh g^{-1} with 96.8 % capacity retention. This is probably due to the well-formed layered structure, as confirmed by the XRD result (Table 2), low cation mixing, and also uniform particle distribution.

In addition, to improve the rate capability of T80 (Figure 6(d)), a current density corresponding to a rate from 1 C to 15 C was applied for the 5$^{\text{th}}$ cycles. With increasing current, the capacity was decreased progressively and the capacity of T80 at 15 C was only 23 mAh g^{-1} after the 5$^{\text{th}}$ cycle. However, almost no capacity decay was observed when the current rate returned to 3 C, suggesting the capacity decrease at high rates was mainly due to the kinetic barrier [42]. Therefore, in this study, we used the 3C rate as the official scan rate for the electrochemical measurements.

Table 4. *Electrochemical performance of LiNi$_{0.3}$Mn$_{0.3}$Co$_{0.3}$Ti$_{0.1}$O$_2$ cathode materials*

Cycles	Capacity, mAh g^{-1}							
	T65		T70		T75		T80	
	Charge	Discharge	Charge	Discharge	Charge	Discharge	Charge	Discharge
1$^{\text{st}}$ cycle	134.1	125.4	146.1	142.5	154.6	142.5	159.4	148.6
2$^{\text{nd}}$ cycle	125.8	125.3	142.5	141.3	142.5	142.5	147.3	147.3
10$^{\text{th}}$ cycle	123.2	121.9	141.3	134.1	140.1	140.1	144.9	146.1
20$^{\text{th}}$ cycle	120.4	118.4	140.1	140.1	137.7	137.7	143.7	144.93
30$^{\text{th}}$ cycle	103.2	103.4	136.5	136.5	136.5	136.5	142.5	143.7
Capacity retention after 2$^{\text{nd}}$ cycle, %	99.9		99.2		100		99.1	
Capacity retention after 30$^{\text{th}}$ cycle, %	82.5		95.8		95.8		96.8	
Efficiency, %	93.5		97.5		92.2		93.2	

Conclusion

In summary, NMCT materials calcined at different temperatures were successfully prepared *via* the combustion method. Rietveld refinements reveal that annealing temperature has a significant effect on the structural parameters of cathode materials. Refinements revealed that T80 material has the best structural integrity by having larger parameters of the c-axis, the lowest cation mixing, and a larger atomic distance of Li-O, which makes this material capable of possessing excellent electrochemical performance behavior compared to the other samples. The SEM result shows the crystallite size increasing with increasing calcination temperatures, indicating that high tempera-tures may promote the formation of more ordered layered structures, and we can see the distribution of the particles is more uniform for T80 material. Furthermore, T80 material shows a smaller ΔE value, indicating better electrode reaction kinetics and rate performance, promising superior electrochemical performance. So, in this case, this material demonstrated excellent cycling stability, with a higher initial discharge capacity of 148.6 mhA g^{-1} and capacity retention of 96.8 %

after 30th cycles, as well as excellent rate capability. The above-mentioned results indicate that T80 material can promote electrochemical performance tremendously and become a potential cathode for Li-ion battery applications. This work also demonstrates that different annealing temperatures have a synergistic effect on the structure, improving the stability and electrochemical performance of NMCT.

Conflicts of Interest: *The authors declare no conflict of interest.*

References

[1]   M. Greenwood, M. Wentker, J. Leker, A region-specific raw material and lithium-ion battery criticality methodology with an assessment of NMC cathode technology, *Applied Energy* **301** (2021) 117512. https://doi.org/10.1016/j.apenergy.2021.117512

[2]   J. Liu, J. Wang, Y. Ni, K. Zhang, F. Cheng, J Chen, Recent breakthroughs and perspectives of high-energy layered oxide cathode materials for lithium ion batteries, *Materials Today* **43** (2021) 132-145. https://doi.org/10.1016/j.mattod.2020.10.028

[3]   S. Lee, T. Lee, High performance hybrid supercapacitors with $LiNi_{1/3}Mn_{1/3}Co_{1/3}O_2$/activated carbon cathode and activated carbon anode, *International Journal of Hydrogen Energy* **43** (2018) 15365-15369. https://doi.org/10.1016/j.ijhydene.2018.06.089

[4]   W. Ahn, S.N. Lim, K.N. Jung, S.H. Yeon, K.B. Kim, H.S. Song, K.H. Shin, Combustion-synthesized $LiNi_{0.6}Mn_{0.2}Co_{0.2}O_2$ as cathode material for lithium ion batteries, *Journal of Alloys and Compounds* **609** (2014) 143-149. http://dx.doi.org/10.1016/j.jallcom.2014.03.123

[5]   J. Ahn, E.K. Jang, S. Yoon, S. Lee, S. Sung, D. Kim, K. Y. Cho, Ultrathin ZrO on $LiNi_{0.5}Mn_{0.3}Co_{0.2}O_2$ electrode surface via atomic layer deposition for high-voltage operation in lithium-ion batteries *Applied Surface Science* **484** (2019) 701-709. https://doi.org/10.1016/j.apsusc.2019.04.123

[6]   X. Yan, L. Zhang, J. Lu, Improve safety of high energy density $LiNi_{1/3}Mn_{1/3}Co_{1/3}O_2$/graphite battery using organosilicon electrolyte, *Electrochimica Acta* **296** (2019) 149-154. https://doi.org/10.1016/j.electacta.2018.11.036

[7]   P. Kaur, K. Singh, Review of perovskite-structure related cathode materials for solid oxide fuel cells, *Ceramics International* **46** (2020) 5521-5535. https://doi.org/10.1016/j.ceramint.2019.11.066

[8]   Y. Xi, Y. Liu, D. Zhang, S. Jin, R. Zhang, M. Jin, Comparative study of the electrochemical performance of $LiNi_{0.5}Mn_{0.3}Co_{0.2}O_2$ and $LiNi_{0.8}Mn_{0.1}Co_{0.1}O_2$ cathode materials for lithium ion batteries, *Solid State Ionics* **327** (2018) 27-31. https://doi.org/10.1016/j.ssi.2018.10.020

[9]   L. Li, Q. Yao, Z. Chen, L. Song, T. Xie, H. Zhu, J. Duan, K. Zhang, Effects of lithium-active manganese trioxide coating on the structural and electrochemical characteristics of $LiNi_{0.5}Co_{0.2}Mn_{0.3}O_2$ as cathode materials for lithium ion battery*, Journal of Alloys and Compounds* **650** (2015) 684-691. http://dx.doi.org/10.1016/j.jallcom.2015.08.041

[10] E. Shinova, R. Stoyanova, E. Zhecheva, G.F. Ortiz, P. Lavela, J.L. Tirado, Cationic distribution and electrochemical performance of on $LiNi_{1/3}Mn_{1/3}Co_{1/3}O_2$ electrodes for lithium-ion batteries, *Solid State Ionics* **179** (2008) 2198-2208. https://doi.org/10.1016/j.ssi.2008.07.026

[11] T. Li, X. Li, Z. Wang, H. Guo, W. Peng, K. Zeng, Electrochemical properties of $LiNi_{0.6}Co_{0.2}Mn_{0.2}O_2$ as cathode material for Li-ion batteries prepared by ultrasonic spray

pyrolysis, *Materials Letters* **159** (2015) 39-42.
http://dx.doi.org/10.1016/j.matlet.2015.06.075

[12]   J. Zeng, C. Hai, X. Ren, X. Li, Y. Shen, O. Dong, L. Zhang, Y. Sun, L. Ma, X. Zhang, S. Dong, Y. Zhou, Facile triethanolamine-assisted combustion synthesized layered LiNi$_{1/3}$Mn$_{1/3}$Co$_{1/3}$O$_2$ cathode materials with enhanced electrochemical performance for lithium-ion batteries, *Journal of Alloys and Compounds* **735** (2018) 1977-1985.
https://doi.org/10.1016/j.jallcom.2017.11.321

[13]   N. Zhao, J. Chen, Z. Liu, K. Ban, W. Duan, Porous LiNi$_{1/3}$Mn$_{1/3}$Co$_{1/3}$O$_2$ microsheets assembled with single crystal nanoparticles as cathode materials for lithium ion batteries, *Journal of Alloys and Compounds* **768** (2018) 782-88. https://doi.org/10.1016/j.jallcom.2018.07.268

[14]   D. Ren, Y. Yang, L. Shen, R. Zeng, H.D. Abrunan, Ni-rich LiNi$_{0.88}$Mn$_{0.06}$Co$_{0.06}$O$_2$ cathode interwoven by carbon fiber with improved rate capability and stability, *Journal of Power Sources* **447** (2020) 227344. https://doi.org/10.1016/j.jpowsour.2019.227344

[15]   M. Li, J. Lu, Z. Chen, K. Amine, 30 Years of Lithium-Ion Batteries, *Advanced Materials* **30** (2018) 1800561. https://doi.org/10.1002/adma.201800561

[16]   V. Paulraj, K. Vediappan, K.K. Bharathi, Phase-surface enabled electrochemical properties and room temperature work function of LiNi$_{1/3}$Mn$_{1/3}$Co$_{1/3}$O$_2$ cathode thin films, *Chemical Physics Letters* **761** (2020) 138074. https://doi.org/10.1016/j.cplett.2020.138074

[17]   M. Eilers-Rethwisch, M. Winter, F.M. Schappacher, Synthesis, electrochemical investigation and structural analysis of doped Li[Ni$_{0.6}$ Mn$_{0.2}$Co$_{0.2-x}$$M_x$]O$_2$ (*x* = 0, 0.05; *M*= Al, Fe, Sn) cathode materials, *Journal of Power Sources* **387** (2018) 101-107.
https://doi.org/10.1016/j.jpowsour.2018.02.080

[18]   Z. Zhang, J. Qiu, M. Yu, C. Jin, B. Yang, G. Guo, Performance of Al-doped LiNi$_{1/3}$Mn$_{1/3}$Co$_{1/3}$O$_2$ synthesized from spent lithium ion batteries by sol-gel method, *Vacuum* **172** (2020) 109105. https://doi.org/10.1016/j.vacuum.2019.109105

[19]   P. B. Samarasingha, A. Wijayasinghe, M. Behm, L. Dissanayake, G. Lindbergh, Developments of cathode materials for lithium ion rechargeable batteries on the system Li[Ni$_{1/3}$ Mn$_{1/3}$Co$_{1/3-x}$M$_x$]O$_2$, (M =Mg, Fe, l and *x* = 0.00 to 0.33), *Solid State Ionics* **268** (2014) 226-230.
http://dx.doi.org/10.1016/j.ssi.2014.07.012

[20]   S. Wang, Y. Li, J. Wu, B. Zheng, M.J. McDonald, Y. Yang, Toward a stabilized lattice framework and surface structure of layered lithium-rich cathode materials with Ti modification, *Physical Chemistry Chemical Physics* **17** (2015) 10151.
https://doi.org/10.1039/C5CP00853K

[21]   D. Zhang, Y. Liu, L. Wu, L. Feng, S. Jin, R. Zhang, M. Jin, Effect of Ti ion doping on electrochemical performance of Ni-rich LiNi$_{0.8}$Co$_{0.1}$Mn$_{0.1}$O$_2$ cathode material, *Electrochimica Acta* **328** (2019) 135086. https://doi.org/10.1016/j.electacta.2019.135086

[22]   X. Yang, C. Bao, L. Xie, L. Zhu, X. Cao, Preparation of LiNi$_{1/3}$Mn$_{1/3}$Co$_{1/3}$O$_2$ polytriphenylamine cathode composites with enhanced electrochemical performances towards reversible lithium storage, *Ceramics International* **45** (2019) 9726-9735.
https://doi.org/10.1016/j.ceramint.2019.02.007

[23]   Y. Fang, Y. Huang, W. Tong, Y. Cai, X. Wang, Y. Guo, D. Jia, J. Zong, Synthesis of hollow peanut-like hierarchical mesoporous LiNi$_{1/3}$Mn$_{1/3}$Co$_{1/3}$O$_2$ cathode materials with exceptional cycle performance for lithium-ion batteries by a simple self-template solid state method, *Journal of Alloys and Compounds* **743** (2018) 707-715.
https://doi.org/10.1016/j.jallcom.2018.01.257

[24]   Q. Su, Y. Li, L. Li, W. Li, G. Cao, L. Xue, J. Li, X. Cao, Synthesis and electrochemical properties of LiNi$_{1/3}$Mn$_{1/3}$Co$_{1/3}$O$_2$ via an original wet-chemical route for high voltage Li-ion batteries, *Materials Letters* **198** (2017) 180-183. http://dx.doi.org/10.1016/j.matlet.2017.03.130

[25] Q. Jing, J. Zhang, C. Yang, Y. Chen, A novel and practical hydrothermal method for synthesizing $LiNi_{1/3}Mn_{1/3}Co_{1/3}O_2$ cathode material, *Ceramics International* **46** (2020) 20020-20026. https://doi.org/10.1016/j.ceramint.2020.05.073

[26] W. Cho, J. H. So, K. Lee, M. Lee, H. Kim, J. Yu, Y. Kim, K. J. Kim, Improved particle hardness of Ti-doped $LiNi_{1/3}Mn_{1/3}Co_{1/3-x}Ti_xO_2$ as high-voltage cathode material for lithium-ion batteries, *Journal of Physics and Chemistry of Solids* **123** (2018) 271-278. https://doi.org/10.1016/j.jpcs.2018.08.008

[27] Y. Zhang, Z. B. Wang, J. Lei, F.F. Li, J. Wu, X.G. Zhang, F.D. Yu, K. Ke, Investigation on performance of $Li(Ni_{0.5}Co_{0.2}Mn_{0.3})1-xTi_xO_2$ cathode materials for lithium-ion battery, *Ceramics International* **41** (2015) 9069-9077. http://dx.doi.org/10.1016/j.ceramint.2015.03.280

[28] S. Refly, O. Floweri, T.R. Mayangsari, A.H. Aimon, F. Iskandar, Green recycle processing of cathode active material from $LiNi_{1/3}Mn_{1/3}Co_{1/3}O_2$ (NMC 111) battery waste through citric acid leaching and oxalate co-precipitation process, *Materials Today: Proceedings* **44** (2021) 3378-3380. https://doi.org/10.1016/j.matpr.2020.11.664

[29] R. Tian, J. Su, Z. Ma, D. Song, X. Shi, H. Zhang, C. Li, L. Zhang, Influences of surface Al concentration on the structure and electrochemical performance of core-shell $LiNi_{0.8}Co_{0.15}Al_{0.05}O_2$ cathode material, *Electrochimica Acta* **337** (2020) 135769. https://doi.org/10.1016/j.electacta.2020.135769

[30] C. Li, Q. Hou, S. Li, F. Tang, P. Wang, Synthesis and properties of nanostructures $LiNi_{1/3}Mn_{1/3}Co_{1/3}O_2$ as cathode with lithium bis(oxalate)borate-based electrolyte to improve cycle performance in Li-ion battery, *Journal of Alloys and Compounds* **723** (2017) 887-893. http://dx.doi.org/10.1016/j.jallcom.2017.06.151

[31] B. Ramkumar, S. Yuvaraj, S. Surendran, K. Pandi, H.V. Ramasamy, Y.S. Lee, R.K. Selvan, Synthesis and characterization of carbon coated $LiNi_{1/3}Mn_{1/3}Co_{1/3}O_2$ and bio-mass derived graphene like porous carbon electrodes for aqueous Li-ion hybrid supercapacitor, *Journal of Physics and Chemistry of Solids* **112** (2018) 270-279. https://doi.org/10.1016/j.jpcs.2017.09.012

[32] A. Iqbal, D. Li, Systematic study of the effect of calcination temperature and Li/M molar ratio on high performance Ni-rich layered $LiNi_{0.9}Co_{0.1}O_2$ cathode materials, *Chemical Physics Letters* **720** (2019) 97-106. https://doi.org/10.1016/j.cplett.2019.01.044

[33] J. Liu, W. Qiu, L. Yu, H. Zhao, T. Li, Synthesis and electrochemical characterization of layered $LiNi_{1/3}Mn_{1/3}Co_{1/3}O_2$ cathode materials by low-temperature solid-state reaction, *Journal of Alloys and Compounds* **449** (2008) 326-330. https://doi.org/10.1016/j.jallcom.2006.01.149

[34] C. Lu, S. Yang, H. Wu, Y. Zhang, X. Yang, T. Liang, Enhanced electrochemical performance of Li-rich $Li_{1.2}Mn_{0.52}Co_{0.08}Ni_{0.2}O_2$ cathode materials for Li-ion batteries by vanadium doping, *Elecrochimica Acta* **209** (2016) 448-445. http://dx.doi.org/10.1016/j.electacta.2016.05.119

[35] M.F. Kasim, W.A.H.W. Azizan, K. Elong, N. Kamarudin, M.K. Yaakob, N. Badar, Enhancing the structural stability and capacity retention of Ni-rich $LiNi_{0.7}Co_{0.3}O_2$ cathode materials via Ti doping for rechargeable Li-ion batteries: Experimental and computational approaches, *Journal of Alloys and Compounds* **888** (2021) 161559. https://doi.org/10.1016/j.jallcom.2021.161559

[36] W.A.H.W. Azizan, M.F. Kasim, K. Elong, R. Rusdi, R.M. Rosnan, N. Kamarulzaman, Effects of Al-dopant at Ni or Co sites in $LiNi_{0.6}Co_{0.3}Ti_{0.1}O_2$ on interlayers slabs (Li-O) and intralayer slabs (TM-O) and their influence on the electrochemical performance of cathode materials, *RSC Advances* **10** (2020) 40291. https://doi.org/10.1039/D0RA07434A

[37] X. Chen, Y. Tang, C. Fan, S. Han, A high stabilized single crystalline nickel-rich $LiNi_{0.8}Co_{0.1}Mn_{0.1}O_2$ cathode through a novel surface spinel-phase modification, *Electrochimica Acta* **341** (2020) 136075. https://doi.org/10.1016/j.electacta.2020.136075

[38]   J. Zheng, W. Zhou, Y. Ma, H. Jin, L. Guo, Combustion synthesis of LiNi$_{1/3}$Mn$_{1/3}$Co$_{1/3}$O$_2$ powder with enhanced electrochemical performance in LIBs*, Journal of Alloys and Compounds* **635** (2015) 207-212. http://dx.doi.org/10.1016/j.jallcom.2015.02.114

[39]   S. Mou, K. Huang, M. Guan, X. Ma, J. S. Chen, Y. Xiang, X. Zhang, Reduced energy barrier for Li$^+$ diffusion in LiCoO$_2$ via dual doping of Ba and Ga, *Journal of Power Sources* **505** (2021) 230067. https://doi.org/10.1016/j.jpowsour.2021.230067

[40]   G. Li, Z. Huang, Z. Zuo, Z. Zhang, H. Zhou, Understanding the trace Ti surface doping on promoting the low temperature performance of LiNi$_{1/3}$Mn$_{1/3}$Co$_{1/3}$O$_2$ cathode, *Journal of Power Sources* **281** (2015) 69-76. http://dx.doi.org/10.1016/j.jpowsour.2015.01.173

[41]   Y. Jiang, Y. Bi, M. Liu, Z. Peng, L. Huai, P. Dong, J. Duan, Z. Chen, X. Li, D. Wang, Y. Zhang, Improved stability of Ni-rich cathode by the substitutive cations with stronger bonds, *Electrochimica Acta* **268** (2018) 41-48. https://doi.org/10.1016/j.electacta.2018.01.119

[42]   Y. Wei, J. Zheng, S. Cui, X. Song, Y. Su, W. Deng, Z. Wu, X. Wang, W. Wang, M. Rao, Y. Lin, C. Wang, K. Amine, F. Pan, Kinetic Tuning of Li-ion Diffusion in Layered Li(Ni$_x$Mn$_y$Co$_z$)O$_2$ *Journal of the American Chemical Society* **137** (26) (2015) 8364-8367. https://doi.org/10.1021/jacs.5b04040